Controls of intermodel uncertainty in land carbon sink projections

Ryan S. Padrón[1], Lukas Gudmundsson[1], Laibao Liu[1], Vincent Humphrey[1,2], Sonia I. Seneviratne[1]

[1]Institute for Atmospheric and Climate Science, Department of Environmental Systems Science, ETH Zurich, Zurich, 8092, Switzerland

5 [2]Department of Geography, University of Zurich, Zurich, Switzerland

Correspondence to: Ryan S. Padrón (ryan.padron@env.ethz.ch)

Abstract. Over the last decades, land ecosystems removed from the atmosphere approximately one third of anthropogenic carbon emissions, highlighting the importance of the evolution of the land carbon sink for projected climate change. Nevertheless, the latest cumulative land carbon sink projections from eleven Earth system models participating in the

10 Coupled Model Intercomparison Project Phase 6 (CMIP6) show large differences, even for a policy-relevant scenario with mean global warming by the end of the century below 2°C relative to preindustrial conditions. We hypothesize that this intermodel uncertainty originates from model differences in the sensitivities of net biome production (NBP) to (i) atmospheric CO_2 concentration, (ii) air temperature and (iii) soil moisture, as well as model differences in average conditions of (iv) air temperature and (v) soil moisture. Using multiple linear regression and a resampling technique, we quantify the

15 individual contributions of these five terms for explaining the cumulative NBP anomaly of each model relative to the multi-model mean. Results indicate a primary role of the response of NBP to interannual temperature and soil moisture variability, followed by the sensitivity to CO_2, and lastly by the average climate conditions, which also show sizeable contributions. We find that the sensitivities of NBP to temperature and soil moisture, particularly in the tropics, dominantly explain the deviations from the ensemble mean of the two models with the lowest carbon sink (ACCESS-ESM1-5 and UKESM1-0-LL)

20 and of the two models with the highest sink (CESM2 and NorESM2-LM). Overall, this study advances our understanding of why land carbon sink projections from Earth system models differ globally and across regions, which can guide efforts to reduce the underlying uncertainties.

1 Introduction

During recent decades, ecosystems on land have taken up approximately one third of anthropogenic carbon emissions to the

25 atmosphere, and are predominantly responsible for the year-to-year variations in the atmospheric carbon growth rate (Friedlingstein et al., 2020). While carbon emissions have been on the rise, land ecosystems have taken up more and more carbon, which has resulted in this approximately constant 30% sink (Canadell et al., 2021). However, it remains unclear to what level this capacity of land to remove carbon from the atmosphere can continue in the coming decades, with evidence pointing towards a less effective sink under increasing cumulative emissions (Gatti et al., 2021; Hubau et al., 2020; Koch et

30 al., 2021; Raupach et al., 2014; Wang et al., 2020; IPCC, 2021). The future evolution of the land carbon sink is crucial to

project how much global warming and consequent climate change Earth will experience given a certain level of greenhouse gas emissions. It is thus linked to policy questions such as how much more carbon can we emit to limit global warming below the 2°C or 1.5°C thresholds decided in the 2015 Paris agreement.

35 The net carbon flux from the atmosphere to the land is denoted as net biome production (NBP), and it is given by the carbon uptake of vegetation (gross primary production (GPP)), minus the losses of carbon to the atmosphere through autotrophic (RA) and heterotrophic respiration (RH), as well as from ecosystem disturbances (DIS) such as fires. The rising atmospheric CO_2 concentration physiologically favors higher GPP, whereas associated warming temperatures tend to increase respiration and can influence all fluxes. In addition to these effects, the relevance of water-carbon interactions for the land carbon cycle

40 has gained recognition in recent years (Canadell et al., 2021; Gentine et al., 2019; Green et al., 2019; Huang et al., 2020; Humphrey et al., 2018; Liu et al., 2020; Novick et al., 2016; Peters et al., 2018; Stocker et al., 2018). Observations indicate a high sensitivity of annual NBP to anomalies in terrestrial water storage at the global scale, which is underestimated by land surface models uncoupled from the atmosphere (Humphrey et al., 2018; Peters et al., 2018). Supporting this finding, Winkler et al. (2021) identified several regions with drought-related observed decreasing trends in leaf area that are underestimated

45 by models. Other factors such as incoming radiation and vapor pressure deficit (air dryness) clearly influence GPP and the land carbon sink (Fu et al., 2022; Grossiord et al., 2020; Humphrey et al., 2021; Novick et al., 2016), nevertheless they are strongly correlated with temperature and soil moisture on monthly or longer time scales. Overall, CO_2 fertilization increases global land NBP, while anthropogenic warming and associated climate change tend to reduce it (Arora et al., 2020; Canadell et al., 2021). Importantly, the response of NBP to interannual climate variability appears to be underestimated by multiple

50 Earth system models, potentially implying a smaller than expected capacity of land to remove carbon from the atmosphere during this century (Fu et al., 2022; Humphrey et al., 2018; Novick et al., 2016; Wang et al., 2020; Winkler et al., 2021).

Projections of the land carbon sink from Earth system models have shown a very substantial intermodel uncertainty since early Coupled Model Intercomparison Projects (CMIPs) (Bonan and Doney, 2018; Friedlingstein et al., 2006) and this

55 continues to be the case for the latest models participating in CMIP6 (Arora et al., 2020; Canadell et al., 2021). While uncertainty in the projections is dominated by these intermodel differences, internal climate variability can also play an important role (Tokarska et al., 2020). Nevertheless, models continue to evolve and represent more processes regarding the land carbon cycle. The representation of the nitrogen cycle in more models was an important step forward going from CMIP5 to CMIP6 (Davies-Barnard et al., 2020). It is often the case that land carbon uptake is reduced when including

60 nitrogen availability as a constraint (Arora et al., 2020; Canadell et al., 2021). In addition, several studies have proposed observational constraints for projections of different land carbon sink components and sensitivities (Cox et al., 2013; Keenan et al., 2021; Liu et al., 2019; Mystakidis et al., 2016, 2017; Schlund et al., 2020; Varney et al., 2020). Despite this progress, land biogeochemical feedbacks with climate change remain a major source of uncertainty for future carbon budgets.

65   The typical framework to study the evolution of the land carbon cycle and associated intermodel uncertainty is based on the carbon-concentration and carbon-climate feedback parameters (Arora et al., 2013, 2020; Friedlingstein et al., 2006). These feedback parameters are estimated from idealized simulations that increase atmospheric CO_2 concentration 1% per year until 2-times (~560 ppm) or 4-times (~1120 ppm) its pre-industrial value and that distinguish between its radiative and biogeochemical effects. Here we consider it important to instead focus on lower concentrations that are compatible with

70   staying below the 2°C global warming level, i.e. 446 ppm by 2100 for the SSP126 scenario (Meinshausen et al., 2020). Another important point is that model differences in the carbon-concentration feedback can arise not only from differences in the effect of CO_2 on GPP, but also from differences in respiration and disturbances which are sensitive to temperature and soil moisture too. Furthermore, differences in the sensitivity of the carbon fluxes to both temperature and soil moisture underlay model differences in the carbon-climate feedback. Arora et al. (2020) provide insights on why the global land

75   carbon feedback parameters differ among models by comparing their changes in vegetation and soil carbon pools, their strength of the CO_2 fertilization effect on GPP, residence time, allocation, and changes in carbon use efficiency globally. To complement these insights and further our understanding of the underlying controls of intermodel uncertainty in land carbon sink projections we directly focus on local responses to CO_2 concentration, temperature, and soil moisture under the SSP126 low emission scenario.

80

    In this study we aim to advance our understanding of the future evolution of the land carbon cycle, primarily for a policy-relevant scenario where global warming is limited to below 2°C. Here we use an ensemble of Earth system models participating in CMIP6, as detailed in section 2. A global and spatially explicit overview of the differences in NBP across models is given in section 3. Section 4 describes across the model ensemble the following five proposed controls of

85   projected cumulative NBP: (i) sensitivity of gross primary production (GPP) to CO_2 concentration, (ii) sensitivity of NBP to air temperature, (iii) sensitivity of NBP to soil moisture, (iv) long-term average temperature, and (v) long-term average soil moisture. In section 5 we quantify the contribution of differences in each of these controls for explaining the intermodel differences in cumulative NBP. Concluding remarks are provided in section 6.

2 Model simulations and characteristics

90   For the main analysis we employ all 11 models participating in CMIP6 that provide NBP, near surface air temperature and layered soil moisture data for the SSP126 scenario (Table S1), which are publicly available at https://esgf-node.llnl.gov/search/cmip6/. Data from all models are regridded to a common a 2.5°×2.5° longitude-latitude grid using second order conservative remapping. The SSP126 scenario is a shared socio-economic pathway based on the world following an ecological transition (Riahi et al., 2017), for which global warming by the end of the century is projected to be

95   less than 2°C relative to preindustrial conditions. In addition, to estimate the sensitivity of GPP to CO_2 concentration, we employ the 1pctCO2-bgc simulations where atmospheric CO_2 increases 1% per year and only its direct physiological effects

on vegetation are considered, while neglecting the radiative effects (Jones et al., 2016). Information from other scenarios is used in some cases to complement the analysis.

100   An overview of the carbon cycle representation in the models analyzed in this study is provided in Table S1. Additional information about the models, except CMCC-ESM2 and EC-Earth3-Veg, is given by Arora et al. (2020). From all 11 models analyzed here, ACCESS-ESM1-5 is the only model that includes a phosphorous cycle in addition to nitrogen, whereas CanESM5, GFDL-ESM4 and IPSL-CM6A-LR do not include a nitrogen cycle, and CNRM-ESM2-1 only has an implicit representation of the nitrogen cycle. Fire emissions are not represented in 4 of the 11 models, namely ACCESS-ESM1-5,

105   CanESM5, IPSL-CM6A-LR and UKESM1-0-LL. Dynamic vegetation cover is only modeled by EC-Earth3-Veg, GFDL-ESM4, MPI-ESM1-2-LR and UKESM1-0-LL. In addition, soil moisture storage capacity and discretization of soil layers can be very different across models (Table S2). To increase comparability, here we compute soil moisture down to a depth of 30 cm for every model by summing the moisture of all corresponding layers. For cases when the 30-cm depth threshold is within the boundaries of a model layer, we assume that the moisture in the layer is distributed uniformly with depth and

110   account proportionally for the moisture until the 30 cm threshold.

3 Intermodel differences in NBP

The cumulative global land carbon sink projections from eleven Earth system models until the year 2100 show large differences, with an ensemble range between 56 PgC and 207 PgC, and a multi-model mean estimate of 144.7 PgC (Fig. 1). The intermodel standard deviation is 47 PgC, which is approximately 5 times the current annual global anthropogenic

115   emissions. Even though these differences are rather large it is important to note that they are smaller than those corresponding to higher emission scenarios such as SSP585, where the range is approximately 100–700 PgC. Thus, uncertainty increases as we move further away from the current state of the system to higher concentrations of greenhouse gases in the atmosphere. Differences across models are considerably larger than differences across realizations of individual models, which partly represent the internal variability of the system (Fig. S1).

120

Further insights on projected intermodel NBP differences are obtained by decomposing them into differences in GPP, autotrophic and heterotrophic respiration, and disturbances (Fig. S2). There is no clear correspondence between models with higher global land GPP having also higher NBP, given that the loss terms are also generally higher. Moreover, the three models with highest NBP project relatively low GPP, as well as low carbon use efficiency (i.e., CUE = (GPP – RA)/GPP),

125   but heterotrophic respiration and disturbance losses are also low. The CUE ranges from 0.66 for GFDL-ESM4 to 0.41 for EC-Earth3-Veg. GFDL-ESM4 and ACCESS-ESM1-5 have the highest CUE, which is counteracted by the highest disturbance losses in these models, whereas the relatively high CUE of CanESM5, UKESM1-0-LL and MPI-ESM1-2-LR is counteracted by high heterotrophic respiration.
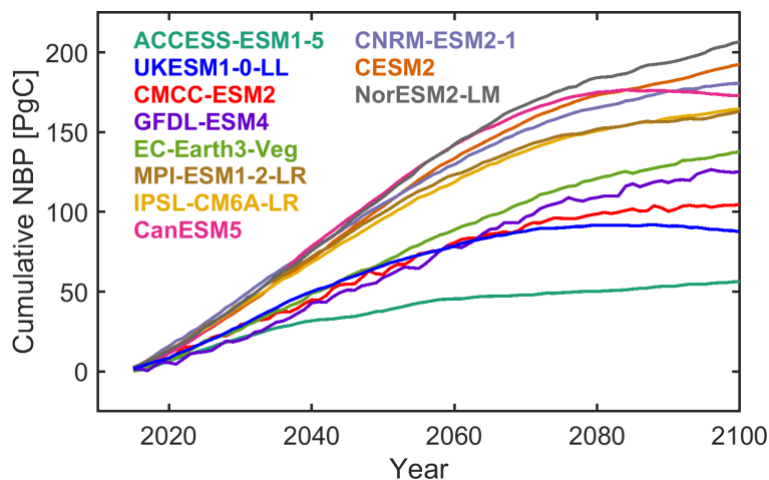
Figure 1: Intermodel differences in projected global land NBP for scenario SSP126. Temporal evolution of projected global land cumulative NBP from individual models. The average value is shown for models with multiple realizations available. If a model does not have information over Greenland, NBP is set to zero. Cumulative global land NBP is estimated by multiplying the area-weighted average NBP times the land surface area excluding Antarctica (135.22E6 km^2).

The maps of cumulative NBP illustrate in more detail the characteristics of the projections from individual models (Fig. 2). Note that there can be models with similar global land NBP as indicated in Fig. 1, even though the underlying spatial distribution is markedly different. Take MPI-ESM1-2-LR and IPSL-CM6A-LR as an example, whereas the tropics – particularly central Africa – are the main sink in the MPI-ESM1-2-LR model, the northern mid and high latitudes contribute most of the sink in IPSL-CM6A-LR. The UKESM1-0-LL and CMCC-ESM2 models also show a very contrasting spatial pattern of cumulative NBP, despite having a relatively similar global land sink magnitude. The local intermodel standard deviation of projected NBP (bottom right panel of Fig. 2) points towards the tropics and boreal forests as the regions with higher discrepancies across models. In addition, models also show marked differences in the magnitude of the detrended interannual variability of NBP (Fig. S3). EC-Earth3-Veg and GFDL-ESM4 have high interannual variability, as well as CMCC-ESM2 particularly over the boreal forests, whereas CESM2 and NorESM2-LM show the least variability.
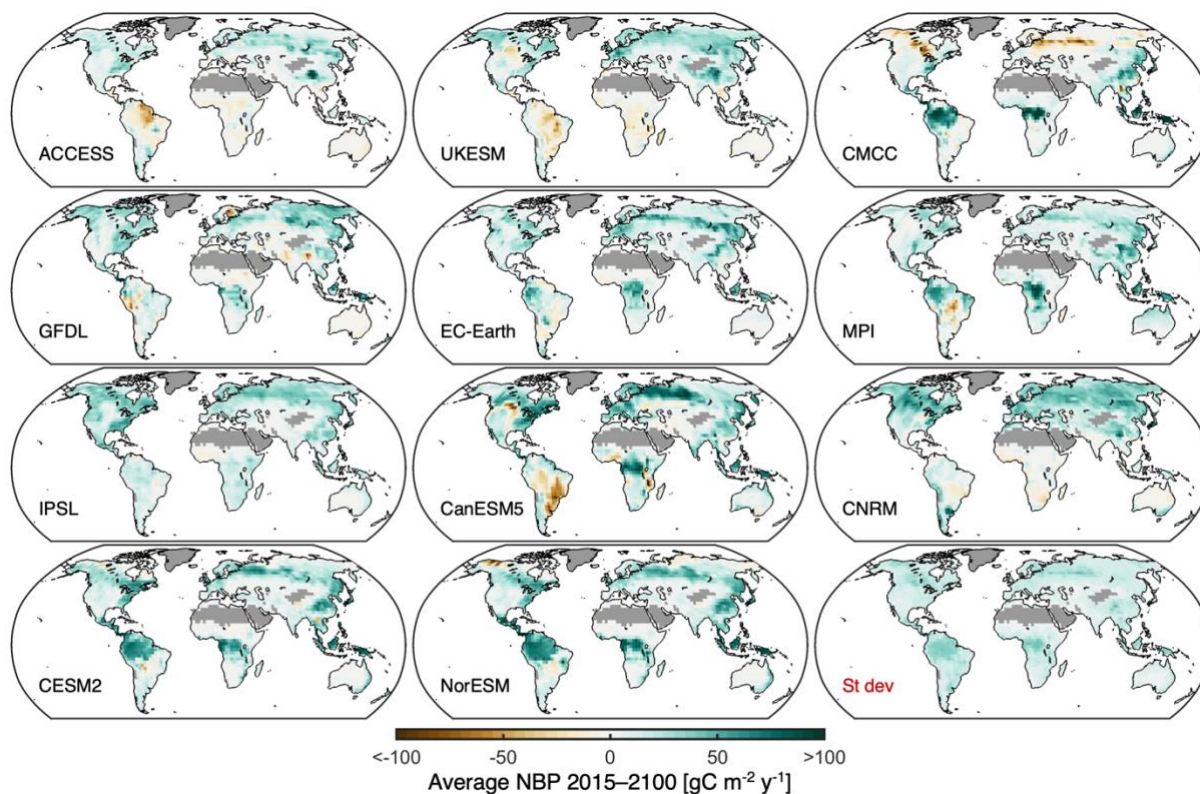
Figure 2: Intermodel differences in regional projected NBP. Maps of average projected NBP during 2015 to 2100 from individual models. The intermodel standard deviation is shown at the bottom right. Greenland and desert regions are masked.

4 Controls of NBP projections

Several factors can influence long-term NBP, with atmospheric CO_2 concentration, air temperature (T) and soil moisture (SM) playing a potentially important role. Here we focus on the sensitivities of NBP to changes in these variables, as well as on the background conditions of T and SM across the model ensemble. Background conditions of atmospheric CO_2 are prescribed and thus identical for all models. Other aspects such as land cover, incoming radiation, air humidity, carbon allocation and nutrient constraints can also be relevant for NBP, however they are addressed only indirectly in this study.

4.1 Sensitivity of GPP to atmospheric CO_2 concentration

The physiological effect of atmospheric CO_2 concentration on NBP is dominated by its influence on GPP. Here we use the 1pctCO2-bgc simulations to estimate the sensitivity of GPP to CO_2 concentration (sCO_2) at every grid cell. These simulations limit confounding effects from changes in temperature and soil moisture as they only account for the biogeochemical effects of rising CO_2. We determine sCO_2 as the slope of the linear regression based on 84 annual values with CO_2 concentration ranging from 350 ppm to 800 ppm. Some of these concentrations are much higher than those from

SSP126, however a large sample is needed to reduce the potential confounding effect of local temperature and soil moisture

160   anomalies from individual years. To further avoid this confounding effect, we compute the regression slope one hundred times after resampling 84 years with replacement from the time series. Finally, the median value of these regression slopes is used as the representative sensitivity from each model. In the case of models with multiple 1pctCO2-bgc simulations the average value is used. Given that no data is available from NorESM2-LM for the 1pctCO2-bgc simulation, we here assume that its sCO_2 is the same as for CESM2 because both share the same land surface model (CLM5).

165

Increasing atmospheric CO_2 concentration favors an overall increase in GPP due to enhanced photosynthesis, although with substantial intermodel differences in sCO_2 particularly in the tropics (Fig. S4). EC-Earth3-Veg, CMCC-ESM2, and ACCESS-ESM1-5 generally exhibit the lowest fertilization effect from atmospheric CO_2, whereas GFDL-ESM4 and MPI-ESM1-2-LR exhibit the highest. Other noteworthy features are the relatively low tropical sCO_2 of IPSL-CM6A-LR and

170   CNRM-ESM2-1, as well as CNRM-ESM2-1 showing the highest sCO_2 in mid and high latitudes.

4.2 Sensitivity of NBP to temperature and soil moisture

Locally, annual warm or cold and wet or dry anomalies can influence annual NBP. The interannual sensitivity of NBP is therefore potentially indicative of the consequences of long-term changes in T and SM on the land carbon sink. In addition, an asymmetry in the response of NBP to a warm (dry) and cold (wet) anomaly of equal magnitude would influence

175   cumulative NBP even if there were no long-term changes in T and SM. In this case too, a different sensitivity would contribute to a difference in cumulative NBP. Thus, model differences in the sensitivity of NBP to interannual variations in T and SM can potentially explain differences in cumulative NBP.

We estimate the sensitivity of NBP to temperature (sT) and soil moisture (sSM) from the detrended time series of annual

180   mean NBP and detrended annual mean warm-season T and SM values from 2015 to 2100 given by the SSP126 simulations. Detrending the time series reduces the potential confounding effect of rising CO_2 concentrations in these simulations. The removed trends are computed using a lowess fit with a 30-year window. In latitudes below 22.5°, we consider all months of the year, whereas in higher latitudes, we focus on the warmer months when vegetation is more active: March–October in the Northern Hemisphere and September–April in the Southern Hemisphere. We define sT and sSM as the covariance of NBP

185   with T and SM, as opposed to the regression slope, to also account for intermodel differences in the interannual variability of T and SM (this is not necessary for sCO_2 given that the interannual variability of CO_2 is prescribed to be the same for all models). In addition to the covariance, we also compute the Pearson correlation to better describe the coupling of NBP with T and SM in the models. In the case of models with multiple simulations the average covariance and average correlation are used.

190

Anomalies in NBP and T are generally negatively correlated (years with higher T lead to lower NBP) throughout the world for most models, except at high latitudes, whereas the opposite is the case for the correlation with SM (years with higher SM lead to higher NBP) (Fig. 3). Nevertheless, there is model disagreement on the sign of the sensitivities in several regions, e.g., southeast Asia, China, western central Europe, central Africa, and throughout the boreal forests. Furthermore, the

195 magnitudes of the correlations and covariances also vary considerably across models (Figs. S5–S8). Some noteworthy features are the highly negative correlation of NBP with T and highly positive correlation with SM over tropical South America for the ACCESS-ESM1-5, UKESM1-0-LL, GFDL-ESM4, EC-Earth3-Veg, and CanESM5 models; the highly positive covariance of NBP with SM over the boreal forests for CMCC-ESM2 and EC-Earth3-Veg; and the negative covariance of NBP with SM in southeast Asia, China, east North America, and southeast Brazil plus Uruguay for UKESM1-
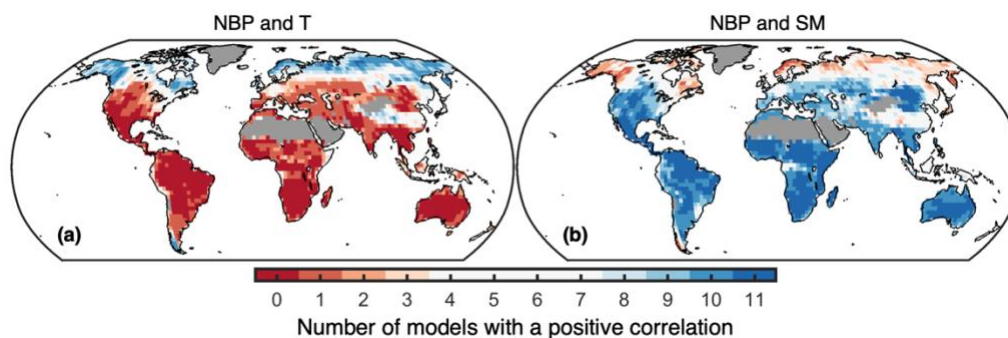
200 0-LL and MPI-ESM1-2-LR.

Figure 3: Model agreement in the sign of the sensitivity of NBP to temperature and soil moisture. (a) Number of models with a positive correlation between detrended NBP and detrended temperature. (b) Number of models with a positive correlation between detrended NBP and detrended soil moisture. Lighter colors indicate higher model disagreement. Greenland and desert regions are masked.

205 Although positive T anomalies often coincide with negative SM anomalies, we find that for most models and across most regions SM explains the detrended interannual variability of NBP better than T, as indicated by the squared correlations (Fig. 4a). For all models, anomalies in SM explain at least 40% of the variability in NBP over a quarter of the land area (excluding deserts and Greenland). Note that in general the interannual correlation of NBP and SM, as well as of NBP and T, is higher precisely where the interannual variability of NBP is higher (Figs. S3, S5 and S6). In addition, to explain the detrended

210 interannual variability of NBP using both T and SM as predictors, we fit a stepwise linear regression. In this case the explained NBP variability increases, reaching an ensemble mean of 57% over a quarter of the land area. Furthermore, we find that over 80% of the land area there is a model majority for which SM is added as the first predictor (Fig. 4b). Notable exceptions are regions with large interannual NBP variability such as parts of the Amazon, central Africa, and southeast Asia, where T is added first for most models. However, note that there is no strong model agreement throughout many

215 regions. Results are consistent when using SM down to 1 m depth instead of 30 cm (Fig. S9). Overall, these findings highlight the importance of explicitly considering the sensitivity to SM, in addition to the sensitivity to T, as a control of intermodel differences in NBP.
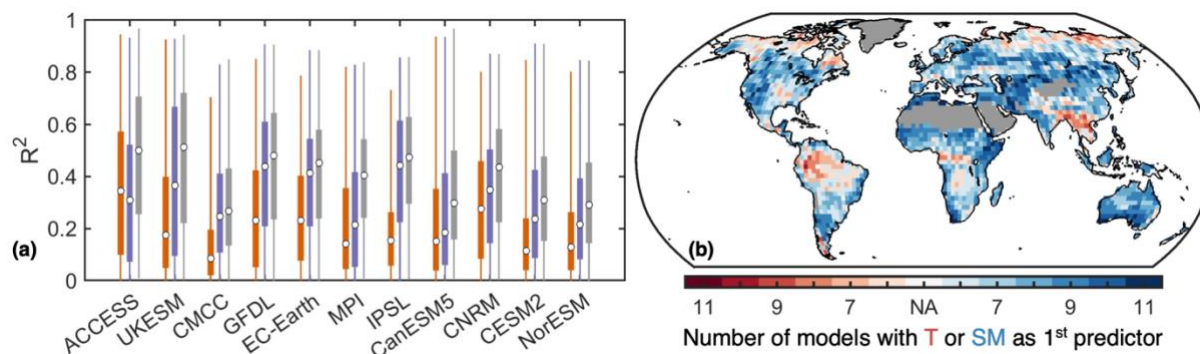
Figure 4: Temperature and soil moisture as controls of the detrended interannual variability of NBP. (a) Area-weighted distribution from all grid cells of the coefficient of determination (R^2) between NBP with T (orange), with SM (purple), and with both T and SM from a stepwise linear regression (grey). The circle indicates the median, the boxes span the interquartile range, and the whiskers the full range. (b) Model agreement at each location where either T or SM is added first to the stepwise linear regression. Greenland and desert regions are masked.

4.3 Average warm-season temperature and soil moisture conditions

The projected long-term average T and SM also influence the cumulative land carbon sink. NBP is negatively affected if conditions are generally too hot, cold, dry, or wet relative to an optimum state. Given that our focus is on cumulative NBP from 2015 to 2100 under the SSP126 scenario, we compute the average warm-season T and SM over the same 86-year period and scenario. We follow the same definition for the warm season as described in section 4.2.

The local intermodel differences in projected average T and top 30 cm SM show a global mean standard deviation of 1.4°C and 14.7 kg m^{-2} over land, with higher values at tropical forests, the United States and Tibet for T, and at very high latitudes for SM (Figs. S10 and S11). GFDL-ESM4, MPI-ESM1-2-LR and IPSL-CM6A-LR generally project lower temperatures, whereas higher temperatures are projected by ACCESS-ESM1-5 and UKESM1-0-LL in the tropics, by CESM2 and NorESM2-LM at mid latitudes, and by CanESM5, CMCC-ESM2, IPSL-CM6A-LR and CNRM-ESM2-1 at high latitudes. NorESM2-LM and CESM2 are clearly the models with highest SM. On the other hand, MPI-ESM1-2-LR, IPSL-CM6A-LR, CanESM5 and UKESM1-0-LL are generally the driest models, as well as ACCESS-ESM1-5 in the tropics.

5 Explaining intermodel differences in cumulative NBP

To assess the effect and relevance of each of the five proposed controls of intermodel differences in the land carbon sink, we compute at each grid cell their correlation with cumulative NBP (Fig. 5). At each grid cell, for example, we correlate the sCO$_2$ values obtained for each of the 11 models with the corresponding 11 values of cumulative NBP from each model. The dominant positive correlation for sCO$_2$, particularly in the extratropics, indicates that models that have a higher CO$_2$ fertilization effect on GPP tend to project higher NBP in these regions. Throughout the tropics, the lack of correlation indicates that intermodel differences in NBP cannot be explained by differences in the strength of the CO$_2$ fertilization effect,

potentially because of other NBP controls. In addition, we find clear positive correlations of cumulative NBP with sT and

245 negative correlations with sSM over multiple regions important for the land carbon sink, such as the Amazon, central Africa, India, China, eastern Australia, Europe, and the boreal forests. This suggests that models that have higher (lower) NBP during warmer (colder) than average years (i.e., higher sT) tend to project higher cumulative NBP in these regions, as do models that have higher (lower) NBP during drier (wetter) than average years (i.e., lower sSM). In other words, models for which annual NBP drops less during hotter and drier years yield higher cumulative NBP (recall Fig. 3). On the other hand,

250 there are also other typically wet regions such as Indonesia and southeast South America where models that have higher (lower) NBP during wetter (drier) than average years (i.e., higher sSM) tend to project higher cumulative NBP. Additionally, we find that higher long-term average warm season T in some models over central Africa, eastern Brazil, the Amazon, as well as central and western United States is associated with lower cumulative NBP. Higher NBP is favored over midwestern North America, the Amazon, European boreal forests, and eastern Australia for models with higher-than-average long-term
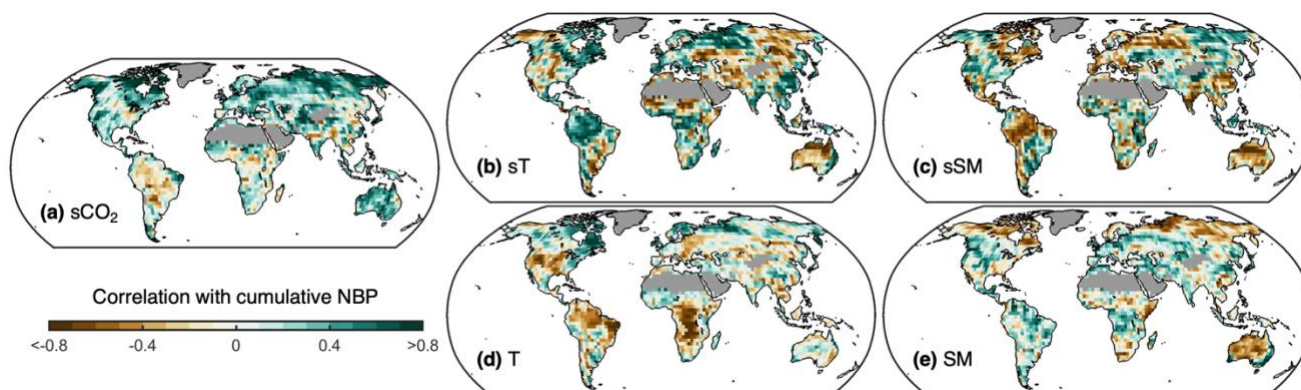
255 mean warm season SM.

Figure 5: Influence of model characteristics on projected cumulative NBP. Pearson correlation at each grid cell between cumulative NBP projected by each Earth system model and their (a) sensitivity to CO_2 concentration (sCO_2), (b) sensitivity to temperature (sT), (c) sensitivity to soil moisture (sSM), (d) long-term warm season average temperature (T), and (e) long-term warm season average soil
260 moisture (SM). For (b) and (c), sT and sSM correspond either to the covariance or to the correlation of detrended annual anomalies of NBP with T and SM, depending on which has the strongest absolute correlation with projected cumulative NBP. Greenland and desert regions are masked.

To quantify the joint contributions of differences in sCO_2, sT, sSM, T and SM for explaining the intermodel differences in projected cumulative NBP, we fit a multiple linear regression at every grid cell. As noted in section 4.2, for sT and sSM we
265 use both the covariance and the correlation of detrended annual anomalies of NBP (NBP_{anom}) with anomalies of warm season temperature (T_{anom}) and soil moisture (SM_{anom}). Therefore, cumulative NBP of each model m is estimated according to Eq. (1):

$$NBP_m = b_0 + b_1 \times sCO_{2_m} + b_2 \times cov(NBP_{anom}, T_{anom})_m + b_3 \times corr(NBP_{anom}, T_{anom})_m +$$

$$b_4 \times cov(NBP_{anom}, SM_{anom})_m + b_5 \times corr(NBP_{anom}, SM_{anom})_m + b_6 \times T_m + b_7 \times SM_m , \qquad (1)$$

10

270   where b_i are the regression coefficients. Given that the number of predictor variables (7) is relatively high, and the sample size is relatively small (11 models), we are likely to obtain a good fit for the regression even if random variables are used instead of the proposed controls. However, a regional spatial coherence on the signs of b_i would only arise if there is an actual relation between NBP and the proposed controls as seen in Fig. 5.

275   Instead of fitting the regression given by Eq. 1 only once at every grid cell using cumulative NBP from 2015 to 2100, we create 200 different bootstrap time series of 86 years by resampling with repetition from all projected years. Then for each of these time series we compute the cumulative NBP of individual models, as well as sT, sSM, T and SM (not sCO_2 as it is estimated from the 1pctCO2-bgc simulations), and finally fit the regression. This bootstrap approach introduces some uncertainty in our estimates of both the proposed controls (Eq. 1, right-hand side) and the cumulative NBP (Eq. 1, left-hand

280   side), which is further propagated into an uncertainty in terms of the regression coefficients b_i. In this way we can provide a likely range for the contribution of each control to explain a given model's anomalous behaviour relative to the ensemble mean cumulative NBP.

The regression estimates capture well the local intermodel variability of cumulative NBP (Fig. S12) and the regression

285   coefficients b_i show regionally coherent signs consistently across the bootstrap realizations (Fig. S13), providing confidence in the robustness of the results. The net aggregated outcome of the local multiple linear regressions (MLR) (Eq. 1) shows good agreement with average projected NBP from individual Earth system models (ESM) at regional and global scales (Fig. 6), with a mean coefficient of determination (R^2) across bootstraps greater than 0.92 in all cases. Thus, most of the intermodel spread in cumulative NBP can be explained from the intermodel spread in the proposed controls. The main

290   discrepancies are an underestimation of the land carbon sink modelled by NorESM2-LM and CanESM5, as well as an overestimation by UKESM1-0-LL, GFDL-ESM4, and IPSL-CM6A-LR. The underestimation for NorESM2-LM arises in the tropics, whereas for CanESM5 it is consistent across all regions. In the case of UKESM1-0-LL and IPSL-CM6A-LR the overestimation from the regression predominantly occurs in the tropics, and to a lesser degree at high latitudes. For GFDL-ESM4 the overestimation is highest at mid latitudes, and it also occurs in the tropics. In addition, for CMCC-ESM2 there is

295   an overestimation at high latitudes that is compensated by an underestimation at the tropics. These differences are likely due to nonlinear responses of NBP that are not captured by the multiple linear regression and/or due to missing relevant controls (e.g., differences in land cover).
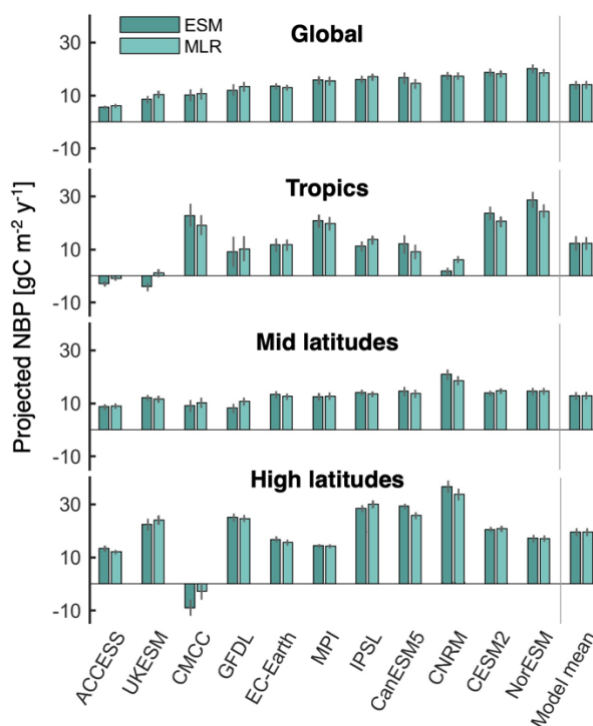
Figure 6: Comparison of average projected NBP from Earth system models (ESM) with the multiple linear regression (MLR)
300   **estimate.** Colored bars indicate the mean from the 200 bootstrap samples, while uncertainty bars span from the 5th to the 95th percentile.
The spatial average is shown for global land, the tropics (22.5°S – 22.5°N), mid latitudes (22.5°N – 47.5°N over North America, 22.5°N –
55°N over Europe and Asia, and > 22.5°S), and high latitudes (> 47.5°N over North America and > 55°N over Europe and Asia).
Greenland and desert regions are omitted. Tropics represent 36% of the considered global land area, mid latitudes 44%, and high latitudes
20%.

305   Given that the regression simulates well projected NBP by the Earth system models, the individual terms of Eq. 1 (i.e., $b_i *$

$control_i$) can be used to quantify the contribution of each proposed control to explain intermodel differences. The

contributions of sT and sSM are obtained by lumping both the correlation and covariance terms. Figure 7 shows how much

each control contributes to explain each model's anomaly in projected NBP relative to the ensemble mean. For example,

33% of the lower-than-average land carbon sink projected by ACCESS-ESM1-5 is due to its low sCO_2 mainly outside the

310   tropics (see Fig. S4), 51% is due to its low sT mainly in the tropics (i.e., lower (higher) NBP during hotter (colder) than

average years compared to other models (see Figs. S5 and S7)), and 17% is due to its high long-term average tropical T (see

Fig. S10), whereas the contributions of SM and sSM are smaller and mostly compensate each other. UKESM1-0-LL also

shows an important contribution towards a relative low land carbon sink from sT and T mainly in the tropics. At the other

end of the spectrum the two models with the highest average projected NBP (CESM2 and NorESM2-LM) show a dominant

315   contribution of sSM in the tropics mainly due to low values in the Amazon and high values in Indonesia (Figs. S6 and S8),

as well as positive contribution due to high long-term SM in the tropics and mid latitudes (see Fig. S11). Other noteworthy

findings are: the strong contribution of sCO_2 at mid and high latitudes to the higher-than-average land carbon sink projected

by CNRM-ESM2-1; the less negative impact of hot temperature anomalies on tropical NBP for CMCC-ESM2, MPI-ESM1-2-LR and IPSL-CM6A-LR together with the relative low long-term average tropical T of the latter two models, which result

320 in positive contributions to average NBP; and the very low average NBP of CMCC-ESM2 at high latitudes resulting from steep drops during years with high T and low SM annual anomalies (sT and sSM contributions). These steep drops in annual NBP are associated with high fire emissions at the boreal forests (Fig. S14), highlighting the importance of adequately representing this process in models given that it can explain much of the differences in average projected NBP. Lastly, we note that CMCC-ESM2, GFDL-ESM4 and EC-Earth3-Veg show the largest uncertainties, particularly in the contributions of

325 sT and sSM. This is related to high fire emissions from individual years which can be in or out of the bootstrap samples, as well as to partial shifts between bootstrap samples in the contributions of sT and sSM due to collinearity.
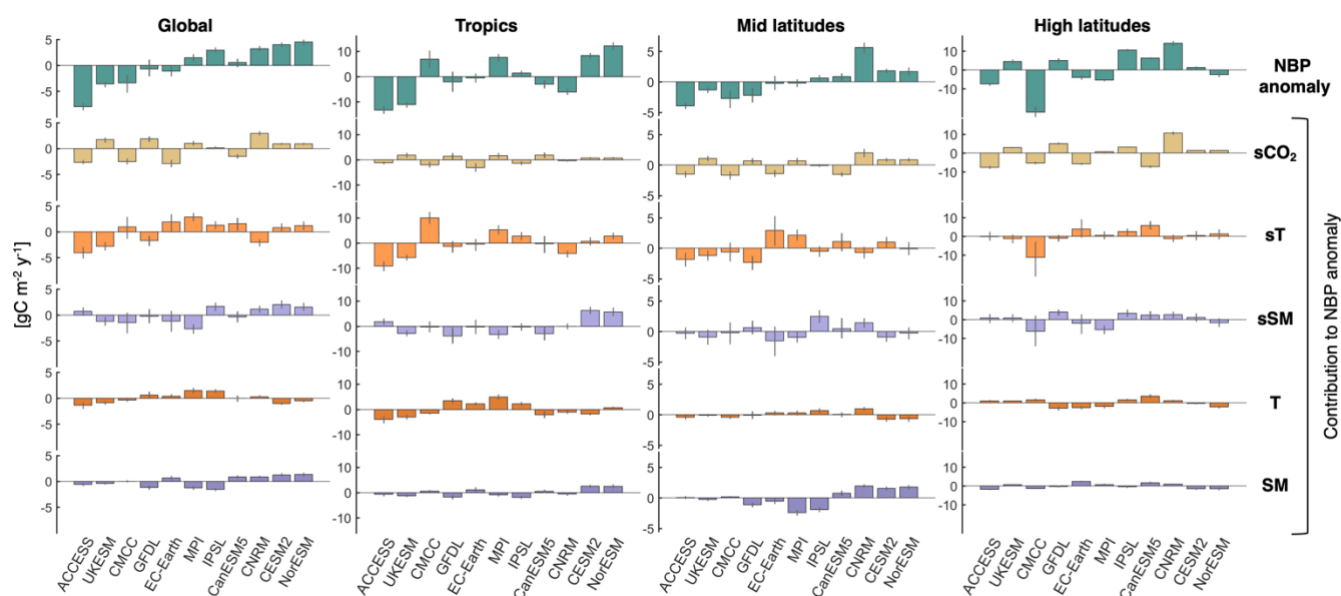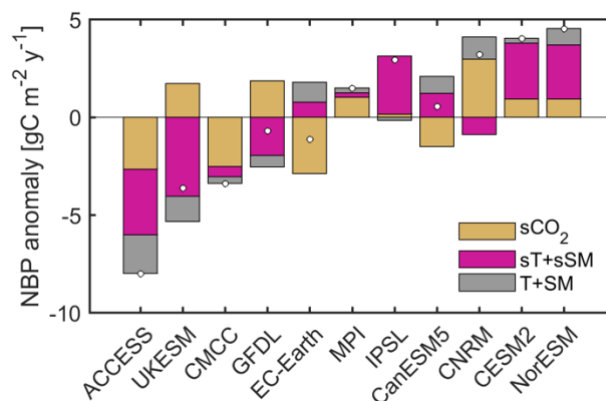

Figure 7: Contributions of the controls to explain the anomaly in average projected NBP from individual models relative to the ensemble mean. Estimates are based on the multiple linear regression. Colored bars indicate the mean from the 200 bootstrap samples,

330 while uncertainty bars span from the 5th to the 95th percentile. The spatial average is shown for global land, the tropics (22.5°S – 22.5°N), mid latitudes (22.5°N – 47.5°N over North America, 22.5°N – 55°N over Europe and Asia, and > 22.5°S), and high latitudes (> 47.5°N over North America and > 55°N over Europe and Asia). Greenland and desert regions are omitted. Tropics represent 36% of the considered global land area, mid latitudes 44%, and high latitudes 20%.

In summary, the contributions of sCO_2, sT and sSM to explain the projected differences in NBP are of similar magnitude,

335 whereas those of T and SM are generally smaller. The overall intermodel standard deviation of global land projected NBP based on the regression estimates is 3.86 gC m^{-2} y^{-1} (equivalent to 44.9 PgC during the period 2015–2100), relative to which the intermodel standard deviations of the contributions from the controls are 53.2% for sCO_2, 58.5% for sT, 39.9% for sSM, 24.5% for T and 27.6% for SM. These results highlight the importance of sSM and SM as controls of projected cumulative NBP, in addition to sT and T. Furthermore, the high intermodel standard deviation values for many of the controls suggest

340 that while constraining any individual control would help reduce the spread of the projected land carbon sink, a large

uncertainty would remain. For example, if we are to assume sCO_2 to be locally equal across all models, by summing the contributions from the other controls we find that the intermodel standard deviation of NBP would still be 3.2 gC m^{-2} y^{-1}, i.e., 83% of the original spread.

345 Figure 8 presents a compact overview of the factors explaining intermodel differences in average projected NBP. We group sT with sSM to represent the sensitivity of NBP to interannual climate variability, and T with SM to represent general background climate conditions. This reduces any potential compensating effects in the contributions of sT, sSM, T and SM that could have resulted from the underlying collinearities between these controls. Differences in the sensitivity of NBP to interannual climate variability play a key role, dominantly explaining the projected anomaly for the two models with lowest

350 land carbon sink, as well as for the two models with highest land carbon sink. We consider it important to note here that ACCESS-ESM1-5 and UKESM1-0-LL share the same atmospheric model component, while CESM2 and NorESM2-LM share the same land surface model. Furthermore, the intermodel variability in the contributions of the sensitivity of NBP to climate corresponds to 63.2% of the total NBP intermodel variability. Differences in the strength of the CO_2 fertilization effect are also clearly important, followed by differences in background climate conditions that nevertheless account for

355 more than 15% of the absolute sum of contributions in 7 out of 11 models. These insights are obtained based on the multiple linear regression, so it is worth noting once again that the regression estimates do not fully match the actual differences between models, with the clearest discrepancies being the underestimation of the sink for CanESM5 and the overestimation for IPSL-CM6A-LR, GFDL-ESM4 and UKESM1-0-LL.

360 **Figure 8: Summary of contributions of the controls to explain intermodel differences in average projected global land NBP.** Bars indicate the grouped contributions of sCO_2, sT plus sSM, and T plus SM to the NBP anomaly estimate from the multiple linear regression. Dots indicate the total NBP anomaly based on the multiple linear regression. From left to right models are ordered according to actual increasing projected land carbon sink.

6 Conclusions

365 In this study we focus on projections of the land carbon sink for a policy-relevant scenario with warming below 2°C by the end of the century (i.e., SSP126). Even under this scenario with a relative low concentration of greenhouse gases, there is an

intermodel spread of approximately 150 PgC in cumulative NBP from 2015 to 2100 – equivalent to 15 years of current anthropogenic emissions – which translates into significant uncertainty in the carbon budget remaining to stabilize global temperature below the chosen threshold. We also show that even when two models project a similar global land carbon sink,

370   there can be large and compensating regional differences. Here we identify regions in which models differ the most and assess which are the underlying model characteristics explaining these differences in the cumulative land carbon sink.

We accurately explain model differences in cumulative NBP as a function of their differences in the sensitivity of GPP to CO_2, the sensitivity of NBP to interannual temperature and soil moisture variability, and projected long-term temperature

375   and soil moisture during the warm season. We detail differences in these five controls across the model ensemble and discuss how they influence the land carbon sink projected by each model throughout the globe. In addition, we find that the detrended interannual variability of projected NBP is better explained by soil moisture than temperature in most models and across most regions. A notable exception is the core of the Amazon, where temperature continues to outperform soil moisture. Given the relevance of model differences in the sensitivity of NBP to temperature and soil moisture, it is

380   increasingly important to further disentangle their sensitivities to incoming radiation and vapor pressure deficit.

Our quantification of the factors explaining intermodel differences in projected NBP highlights the dominant role of the response of the land carbon cycle to interannual temperature and soil moisture variability over that of the CO_2 fertilization effect and average climate conditions. This finding provides explicit evidence that improving the representation of the local-

385   scale sensitivity of NBP to interannual climate variability has the potential to reduce uncertainty in long-term projections of the global land carbon sink. However, we also find that the different controls of NBP model spread often have compensating effects, as evidenced by multiple models with an above average CO_2 fertilization effect being more adversely affected by interannual climate variability and vice versa (see instances of opposing contributions of sCO2 and sT + sSM in Fig. 8). Thus, much of the model spread in cumulative NBP would remain even if we would be able to constrain a single control. A

390   noteworthy aspect of this study is to explicitly consider the role of soil moisture when explaining model differences in projected cumulative NBP, as it provides valuable information in addition to temperature. We highlight substantial contributions from model differences in the sensitivity of NBP to interannual soil moisture variability, and to a lesser extent from differences in long-term average soil moisture.

395   In the quest to better understand the future evolution of the land carbon cycle, our detailed insights about why each model projects either a relatively high or low cumulative land carbon sink is a valuable roadmap to reducing uncertainty. Furthermore, our findings emphasize the need for spatially explicit observations of the sensitivity of the land carbon cycle to changes in temperature, soil moisture and CO_2 concentration, among other variables. Fortunately, this is becoming increasingly feasible thanks to progress in estimating carbon fluxes through in-situ observational networks, atmospheric

400 inversions, and remote sensing products. The insights from this study together with those from novel observations are set to pave the way towards more confident projections of the evolution of the land carbon sink.

Code and data availability

The CMIP6 data used in this study are available at https://esgf-node.llnl.gov/search/cmip6/. Detailed inputs for the search query are as follows: Source ID: see Table S1; Experiment ID: ssp126, ssp585 and 1pctCO2-bgc; Frequency: mon; Variable:
405 nbp, tas, mrsol, gpp, ra, rh, fFire.

Scripts used for the analysis are available during review at: https://polybox.ethz.ch/index.php/s/ElMQLCRRqaf4iwa.

Author contributions

RSP, LG, and SIS conceived the idea and designed the study. RSP processed the CMIP6 data, performed the analysis and
410 wrote the paper with periodic suggestions from all authors. All authors discussed the results, read, and reviewed the paper.

420 **References**

Arora, V. K., Boer, G. J., Friedlingstein, P., Eby, M., Jones, C. D., Christian, J. R., Bonan, G., Bopp, L., Brovkin, V., Cadule, P., Hajima, T., Ilyina, T., Lindsay, K., Tjiputra, J. F. and Wu, T.: Carbon–Concentration and Carbon–Climate Feedbacks in CMIP5 Earth System Models, J. Clim., 26(15), 5289–5314, doi:10.1175/JCLI-D-12-00494.1, 2013.

Arora, V. K., Katavouta, A., Williams, R. G., Jones, C. D., Brovkin, V., Friedlingstein, P., Schwinger, J., Bopp, L., Boucher,
425 O., Cadule, P., Chamberlain, M. A., Christian, J. R., Delire, C., Fisher, R. A., Hajima, T., Ilyina, T., Joetzjer, E., Kawamiya, M., Koven, C. D., Krasting, J. P., Law, R. M., Lawrence, D. M., Lenton, A., Lindsay, K., Pongratz, J., Raddatz, T., Séférian,

R., Tachiiri, K., Tjiputra, J. F., Wiltshire, A., Wu, T. and Ziehn, T.: Carbon–concentration and carbon–climate feedbacks in CMIP6 models and their comparison to CMIP5 models, Biogeosciences, 17(16), 4173–4222, doi:10.5194/bg-17-4173-2020, 2020.

430   Bonan, G. B. and Doney, S. C.: Climate, ecosystems, and planetary futures: The challenge to predict life in Earth system models, Science (80-.)., 359(6375), doi:10.1126/SCIENCE.AAM8328, 2018.

Canadell, J. G., Monteiro, P. M. S., Costa, M. H., Cotrim da Cunha, L., Cox, P. M., Eliseev, A. V., Henson, S., Ishii, M., Jaccard, S., Koven, C., Lohila, A., Patra, P. K., Piao, S., Rogelj, J., Syampungani, S., Zaehle, S. and Zickfeld, K.: Global Carbon and other Biogeochemical Cycles and Feedbacks, in Climate Change 2021: The Physical Science Basis.

435   Contribution of Working Group I to the Sixth Assessment Report of the Intergovernmental Panel on Climate Change. [Masson-Delmotte, V., P. Zhai, A. Pirani, S. L. Connors, C. Péan, S. Berger, N. Caud, Y. Chen, L. Goldfarb, M. I. Gomis, M. Huang, K. Leitzell, E. Lonnoy, J.B.R. Matthews, T. K. Maycock, T. Waterfield, O. Yelekçi, R. Yu and B. Zhou (eds.)]. Cambridge University Press., 2021.

Cox, P. M., Pearson, D., Booth, B. B., Friedlingstein, P., Huntingford, C., Jones, C. D. and Luke, C. M.: Sensitivity of
440   tropical carbon to climate change constrained by carbon dioxide variability, Nature, 494(7437), 341–344, doi:10.1038/nature11882, 2013.

Davies-Barnard, T., Meyerholt, J., Zaehle, S., Friedlingstein, P., Brovkin, V., Fan, Y., Fisher, R. A., Jones, C. D., Lee, H., Peano, D., Smith, B., Wårlind, D. and Wiltshire, A. J.: Nitrogen cycling in CMIP6 land surface models: progress and limitations, Biogeosciences, 17(20), 5129–5148, doi:10.5194/bg-17-5129-2020, 2020.

445   Friedlingstein, P., Cox, P., Betts, R., Bopp, L., von Bloh, W., Brovkin, V., Cadule, P., Doney, S., Eby, M., Fung, I., Bala, G., John, J., Jones, C., Joos, F., Kato, T., Kawamiya, M., Knorr, W., Lindsay, K., Matthews, H. D., Raddatz, T., Rayner, P., Reick, C., Roeckner, E., Schnitzler, K.-G., Schnur, R., Strassmann, K., Weaver, A. J., Yoshikawa, C. and Zeng, N.: Climate–Carbon Cycle Feedback Analysis: Results from the C4MIP Model Intercomparison, J. Clim., 19(14), 3337–3353, doi:10.1175/JCLI3800.1, 2006.

450   Friedlingstein, P., O'Sullivan, M., Jones, M. W., Andrew, R. M., Hauck, J., Olsen, A., Peters, G. P., Peters, W., Pongratz, J., Sitch, S., Le Quéré, C., Canadell, J. G., Ciais, P., Jackson, R. B., Alin, S., Aragão, L. E. O. C., Arneth, A., Arora, V., Bates, N. R., Becker, M., Benoit-Cattin, A., Bittig, H. C., Bopp, L., Bultan, S., Chandra, N., Chevallier, F., Chini, L. P., Evans, W., Florentie, L., Forster, P. M., Gasser, T., Gehlen, M., Gilfillan, D., Gkritzalis, T., Gregor, L., Gruber, N., Harris, I., Hartung, K., Haverd, V., Houghton, R. A., Ilyina, T., Jain, A. K., Joetzjer, E., Kadono, K., Kato, E., Kitidis, V., Korsbakken, J. I.,
455   Landschützer, P., Lefèvre, N., Lenton, A., Lienert, S., Liu, Z., Lombardozzi, D., Marland, G., Metzl, N., Munro, D. R., Nabel, J. E. M. S., Nakaoka, S.-I., Niwa, Y., O'Brien, K., Ono, T., Palmer, P. I., Pierrot, D., Poulter, B., Resplandy, L., Robertson, E., Rödenbeck, C., Schwinger, J., Séférian, R., Skjelvan, I., Smith, A. J. P., Sutton, A. J., Tanhua, T., Tans, P. P., Tian, H., Tilbrook, B., van der Werf, G., Vuichard, N., Walker, A. P., Wanninkhof, R., Watson, A. J., Willis, D., Wiltshire, A. J., Yuan, W., Yue, X. and Zaehle, S.: Global Carbon Budget 2020, Earth Syst. Sci. Data, 12(4), 3269–3340,
460   doi:10.5194/essd-12-3269-2020, 2020.

Fu, Z., Ciais, P., Prentice, I. C., Gentine, P., Makowski, D., Bastos, A., Luo, X., Green, J. K., Stoy, P. C., Yang, H. and Hajima, T.: Atmospheric dryness reduces photosynthesis along a large range of soil water deficits, Nat. Commun., 13(1), 989, doi:10.1038/s41467-022-28652-7, 2022.

Gatti, L. V., Basso, L. S., Miller, J. B., Gloor, M., Gatti Domingues, L., Cassol, H. L. G., Tejada, G., Aragão, L. E. O. C.,
465   Nobre, C., Peters, W., Marani, L., Arai, E., Sanches, A. H., Corrêa, S. M., Anderson, L., Von Randow, C., Correia, C. S. C., Crispim, S. P. and Neves, R. A. L.: Amazonia as a carbon source linked to deforestation and climate change, Nature, 595(7867), 388–393, doi:10.1038/s41586-021-03629-6, 2021.

Gentine, P., Green, J. K., Guérin, M., Humphrey, V., Seneviratne, S. I., Zhang, Y. and Zhou, S.: Coupling between the terrestrial carbon and water cycles-a review, Environ. Res. Lett., doi:10.1088/1748-9326/ab22d6, 2019.

470   Green, J. K., Seneviratne, S. I., Berg, A. M., Findell, K. L., Hagemann, S., Lawrence, D. M. and Gentine, P.: Large influence of soil moisture on long-term terrestrial carbon uptake, Nature, 565(7740), 476–479, doi:10.1038/s41586-018-0848-x, 2019.

Grossiord, C., Buckley, T. N., Cernusak, L. A., Novick, K. A., Poulter, B., Siegwolf, R. T. W., Sperry, J. S. and McDowell, N. G.: Plant responses to rising vapor pressure deficit, New Phytol., 226(6), 1550–1566, doi:10.1111/nph.16485, 2020.

Huang, L., Chen, K. and Zhou, M.: Climate change and carbon sink: a bibliometric analysis, Environ. Sci. Pollut. Res.,
475   27(8), 8740–8758, doi:10.1007/s11356-019-07489-6, 2020.

Hubau, W., Lewis, S. L., Phillips, O. L., Affum-Baffoe, K., Beeckman, H., Cuní-Sanchez, A., Daniels, A. K., Ewango, C. E. N., Fauset, S., Mukinzi, J. M., Sheil, D., Sonké, B., Sullivan, M. J. P., Sunderland, T. C. H., Taedoumg, H., Thomas, S. C., White, L. J. T., Abernethy, K. A., Adu-Bredu, S., Amani, C. A., Baker, T. R., Banin, L. F., Baya, F., Begne, S. K., Bennett, A. C., Benedet, F., Bitariho, R., Bocko, Y. E., Boeckx, P., Boundja, P., Brienen, R. J. W., Brncic, T., Chezeaux, E.,
480   Chuyong, G. B., Clark, C. J., Collins, M., Comiskey, J. A., Coomes, D. A., Dargie, G. C., de Haulleville, T., Kamdem, M. N. D., Doucet, J.-L., Esquivel-Muelbert, A., Feldpausch, T. R., Fofanah, A., Foli, E. G., Gilpin, M., Gloor, E., Gonmadje, C., Gourlet-Fleury, S., Hall, J. S., Hamilton, A. C., Harris, D. J., Hart, T. B., Hockemba, M. B. N., Hladik, A., Ifo, S. A., Jeffery, K. J., Jucker, T., Yakusu, E. K., Kearsley, E., Kenfack, D., Koch, A., Leal, M. E., Levesley, A., Lindsell, J. A., Lisingo, J., Lopez-Gonzalez, G., Lovett, J. C., Makana, J.-R., Malhi, Y., Marshall, A. R., Martin, J., Martin, E. H., Mbayu, F. M.,
485   Medjibe, V. P., Mihindou, V., Mitchard, E. T. A., Moore, S., Munishi, P. K. T., Bengone, N. N., Ojo, L., Ondo, F. E., Peh, K. S.-H., Pickavance, G. C., Poulsen, A. D., Poulsen, J. R., Qie, L., Reitsma, J., Rovero, F., Swaine, M. D., Talbot, J., Taplin, J., Taylor, D. M., Thomas, D. W., Toirambe, B., Mukendi, J. T., Tuagben, D., Umunay, P. M., et al.: Asynchronous carbon sink saturation in African and Amazonian tropical forests, Nature, 579(7797), 80–87, doi:10.1038/s41586-020-2035-0, 2020.

490   Humphrey, V., Zscheischler, J., Ciais, P., Gudmundsson, L., Sitch, S. and Seneviratne, S. I.: Sensitivity of atmospheric CO2 growth rate to observed changes in terrestrial water storage, Nature, 560(7720), 628–631, doi:10.1038/s41586-018-0424-4, 2018.

Humphrey, V., Berg, A., Ciais, P., Gentine, P., Jung, M., Reichstein, M., Seneviratne, S. I. and Frankenberg, C.: Soil moisture–atmosphere feedback dominates land carbon uptake variability, Nature, 592(7852), 65–69, doi:10.1038/s41586-

495   021-03325-5, 2021.

IPCC, 2021: Summary for Policymakers. In: *Climate Change 2021: The Physical Science Basis. Contribution of Working Group I to the Sixth Assessment Report of the Intergovernmental Panel on Climate Change* [Masson-Delmotte, V., P. Zhai, A. Pirani, S.L. Connors, C. Péan, S. Berger, N. Caud, Y. Chen, L. Goldfarb, M.I. Gomis, M. Huang, K. Leitzell, E. Lonnoy, J.B.R. Matthews, T.K. Maycock, T. Waterfield, O. Yelekçi, R. Yu, and B. Zhou (eds.)]. In Press.

500   Jones, C. D., Arora, V., Friedlingstein, P., Bopp, L., Brovkin, V., Dunne, J., Graven, H., Hoffman, F., Ilyina, T., John, J. G., Jung, M., Kawamiya, M., Koven, C., Pongratz, J., Raddatz, T., Randerson, J. T. and Zaehle, S.: C4MIP – The Coupled Climate–Carbon Cycle Model Intercomparison Project: experimental protocol for CMIP6, Geosci. Model Dev., 9(8), 2853–2880, doi:10.5194/gmd-9-2853-2016, 2016.

Keenan, T. F., Luo, X., De Kauwe, M. G., Medlyn, B. E., Prentice, I. C., Stocker, B. D., Smith, N. G., Terrer, C., Wang, H.,
505   Zhang, Y. and Zhou, S.: A constraint on historic growth in global photosynthesis due to increasing CO2, Nature, 600(7888), 253–258, doi:10.1038/s41586-021-04096-9, 2021.

Koch, A., Hubau, W. and Lewis, S. L.: Earth System Models Are Not Capturing Present-Day Tropical Forest Carbon Dynamics, Earth's Futur., 9(5), e2020EF001874, doi:10.1029/2020EF001874, 2021.

Liu, L., Gudmundsson, L., Hauser, M., Qin, D., Li, S. and Seneviratne, S. I.: Soil moisture dominates dryness stress on
510   ecosystem production globally, Nat. Commun., 11(1), 4892, doi:10.1038/s41467-020-18631-1, 2020.

Liu, Y., Piao, S., Gasser, T., Ciais, P., Yang, H., Wang, H., Keenan, T. F., Huang, M., Wan, S., Song, J., Wang, K., Janssens, I. A., Peñuelas, J., Huntingford, C., Wang, X., Altaf Arain, M., Fang, Y., Fisher, J. B., Huang, M., Huntzinger, D. N., Ito, A., Jain, A. K., Mao, J., Michalak, A. M., Peng, C., Poulter, B., Schwalm, C., Shi, X., Tian, H., Wei, Y., Zeng, N., Zhu, Q. and Wang, T.: Field-experiment constraints on the enhancement of the terrestrial carbon sink by CO2 fertilization, Nat. Geosci.,
515   12(10), 809–814, doi:10.1038/s41561-019-0436-1, 2019.

Meinshausen, M., Nicholls, Z. R. J., Lewis, J., Gidden, M. J., Vogel, E., Freund, M., Beyerle, U., Gessner, C., Nauels, A., Bauer, N., Canadell, J. G., Daniel, J. S., John, A., Krummel, P. B., Luderer, G., Meinshausen, N., Montzka, S. A., Rayner, P. J., Reimann, S., Smith, S. J., van den Berg, M., Velders, G. J. M., Vollmer, M. K. and Wang, R. H. J.: The shared socio-economic pathway (SSP) greenhouse gas concentrations and their extensions to 2500, Geosci. Model Dev., 13(8), 3571–
520   3605, doi:10.5194/gmd-13-3571-2020, 2020.

Mystakidis, S., Davin, E. L., Gruber, N. and Seneviratne, S. I.: Constraining future terrestrial carbon cycle projections using observation-based water and carbon flux estimates, Glob. Chang. Biol., 22(6), 2198–2215, doi:10.1111/gcb.13217, 2016.

Mystakidis, S., Seneviratne, S. I., Gruber, N. and Davin, E. L.: Hydrological and biogeochemical constraints on terrestrial carbon cycle feedbacks, Environ. Res. Lett., 12(1), 014009, doi:10.1088/1748-9326/12/1/014009, 2017.

525   Novick, K. A., Ficklin, D. L., Stoy, P. C., Williams, C. A., Bohrer, G., Oishi, A. C., Papuga, S. A., Blanken, P. D., Noormets, A., Sulman, B. N., Scott, R. L., Wang, L. and Phillips, R. P.: The increasing importance of atmospheric demand for ecosystem water and carbon fluxes, Nat. Clim. Chang., 6(11), 1023–1027, doi:10.1038/nclimate3114, 2016.

Peters, W., van der Velde, I. R., van Schaik, E., Miller, J. B., Ciais, P., Duarte, H. F., van der Laan-Luijkx, I. T., van der

Molen, M. K., Scholze, M., Schaefer, K., Vidale, P. L., Verhoef, A., Wårlind, D., Zhu, D., Tans, P. P., Vaughn, B. and

530 White, J. W. C.: Increased water-use efficiency and reduced CO2 uptake by plants during droughts at a continental scale, Nat. Geosci., 11(10), 744–748, doi:10.1038/s41561-018-0212-7, 2018.

Raupach, M. R., Gloor, M., Sarmiento, J. L., Canadell, J. G., Frölicher, T. L., Gasser, T., Houghton, R. A., Le Quéré, C. and Trudinger, C. M.: The declining uptake rate of atmospheric CO 2 by land and ocean sinks, Biogeosciences, 11, 3453–3475, doi:10.5194/bg-11-3453-2014, 2014.

535 Riahi, K., van Vuuren, D. P., Kriegler, E., Edmonds, J., O'Neill, B. C., Fujimori, S., Bauer, N., Calvin, K., Dellink, R., Fricko, O., Lutz, W., Popp, A., Cuaresma, J. C., KC, S., Leimbach, M., Jiang, L., Kram, T., Rao, S., Emmerling, J., Ebi, K., Hasegawa, T., Havlik, P., Humpenöder, F., Da Silva, L. A., Smith, S., Stehfest, E., Bosetti, V., Eom, J., Gernaat, D., Masui, T., Rogelj, J., Strefler, J., Drouet, L., Krey, V., Luderer, G., Harmsen, M., Takahashi, K., Baumstark, L., Doelman, J. C., Kainuma, M., Klimont, Z., Marangoni, G., Lotze-Campen, H., Obersteiner, M., Tabeau, A. and Tavoni, M.: The Shared

540 Socioeconomic Pathways and their energy, land use, and greenhouse gas emissions implications: An overview, Glob. Environ. Chang., 42, 153–168, doi:10.1016/J.GLOENVCHA.2016.05.009, 2017.

Schlund, M., Eyring, V., Camps-Valls, G., Friedlingstein, P., Gentine, P. and Reichstein, M.: Constraining Uncertainty in Projected Gross Primary Production With Machine Learning, J. Geophys. Res. Biogeosciences, 125(11), e2019JG005619, doi:10.1029/2019JG005619, 2020.

545 Stocker, B. D., Zscheischler, J., Keenan, T. F., Prentice, I. C., Peñuelas, J. and Seneviratne, S. I.: Quantifying soil moisture impacts on light use efficiency across biomes, New Phytol., 218(4), 1430–1449, doi:10.1111/nph.15123, 2018.

Tokarska, K. B., Arora, V. K., Gillett, N. P., Lehner, F., Rogelj, J., Schleussner, C.-F., Séférian, R. and Knutti, R.: Uncertainty in carbon budget estimates due to internal climate variability, Environ. Res. Lett., doi:10.1088/1748-9326/abaf1b, 2020.

550 Varney, R. M., Chadburn, S. E., Friedlingstein, P., Burke, E. J., Koven, C. D., Hugelius, G. and Cox, P. M.: A spatial emergent constraint on the sensitivity of soil carbon turnover to global warming, Nat. Commun., 11(1), 5544, doi:10.1038/s41467-020-19208-8, 2020.

Wang, S., Zhang, Y., Ju, W., Chen, J. M., Ciais, P., Cescatti, A., Sardans, J., Janssens, I. A., Wu, M., Berry, J. A., Campbell, E., Fernández-Martínez, M., Alkama, R., Sitch, S., Friedlingstein, P., Smith, W. K., Yuan, W., He, W., Lombardozzi, D.,

555 Kautz, M., Zhu, D., Lienert, S., Kato, E., Poulter, B., Sanders, T. G. M., Krüger, I., Wang, R., Zeng, N., Tian, H., Vuichard, N., Jain, A. K., Wiltshire, A., Haverd, V., Goll, D. S. and Peñuelas, J.: Recent global decline of CO2 fertilization effects on vegetation photosynthesis, Science (80-.)., 370(6522), 1295–1300, doi:10.1126/SCIENCE.ABB7772, 2020.

Winkler, A. J., Myneni, R. B., Hannart, A., Sitch, S., Haverd, V., Lombardozzi, D., Arora, V. K., Pongratz, J., Nabel, J. E. M. S., Goll, D. S., Kato, E., Tian, H., Arneth, A., Friedlingstein, P., Jain, A. K., Zaehle, S. and Brovkin, V.: Slowdown of the

560 greening trend in natural vegetation with further rise in atmospheric CO2, Biogeosciences, 18(17), 4985–5010, doi:10.5194/bg-18-4985-2021, 2021.